Giant resonance region of ^{15}N studied by polarized and unpolarized proton capture measurements

H. R. Weller* and R. A. Blue
University of Florida †
and Triangle Universities Nuclear Laboratory, ‡ *Durham, North Carolina 27706*

N. R. Roberson, D. G. Rickel, S. Maripuu, C. P. Cameron, and R. D. Ledford
Duke University
and Triangle Universities Nuclear Laboratory, Duke Station, Durham, North Carolina 27706

D. R. Tilley
North Carolina State University
and Triangle Universities Nuclear Laboratory, Duke Station, Durham, North Carolina 27706
(Received 27 August 1975)

We have measured the cross sections and the analyzing powers for the $^{14}C(\vec{p}, \gamma)^{15}N$ reaction for proton energies from 4.0 to 16.2 MeV. The corresponding range in excitation energies, 13.94 to 25.33 MeV, covers the region of the giant dipole resonance in ^{15}N. The five-angle angular distributions measured with unpolarized and with polarized beams at eight energies over this region were analyzed to determine the magnitudes and relative phases of the transition matrix elements. The analysis included $E1$, $M1$, and $E2$ transitions. The observed $E1$ strength exhausts only about 6% of the classical dipole sum rule. The dominant $E1$ strength is compared to a shell-model calculation which includes 3p-3h excitations. A fairly uniform distribution of $E2$ strength is observed which exhausts about 7% of the total energy-weighted sum rule. Although large uncertainties on this result could allow the existence of a giant $E2$ resonance, the most probable values indicate that no appreciable concentration of $E2$ strength is observed.

[NUCLEAR REACTIONS $^{14}C(\vec{p}, \gamma_0)$; measured $\sigma(E)$, $E=4.0-16.2$ MeV; measured $\sigma(\theta)$ and $A(\theta)$, $E=4.8-13.6$ MeV. ^{15}N deduced T-matrix amplitudes and phases. Compared $E2$ strength to energy-weighted sum rule. Compared $E1$ strength to shell-model calculation. Enriched targets.]

I. INTRODUCTION

Previous experiments have demonstrated the utility of measurements in the giant resonance region of nuclei using polarized proton capture reactions.[1-3] While cross section data alone is usually not sufficient to resolve ambiguities in the magnitudes and phases of the various amplitudes which may contribute to the reaction, analyzing power measurements may provide additional information which can remove these ambiguities. In particular, it may be possible to determine the $E2$ (electric quadrupole) cross section[4] in the region of the giant dipole resonance. This is important in connection with establishing the existence and detailed properties of a possible giant electric quadrupole resonance (GQR). The present evidence for the existence of a GQR comes from inelastic scattering of electrons, protons, ^{3}He nuclei and α particles[5] from intermediate to heavy mass nuclei. Recent (α, α') data[6] have indicated that the GQR becomes quite spread out for nuclei with mass number $A < 40$.

In the case of the light nuclei most of the data relevant to the GQR come from radiative capture measurements. Generally speaking, these results fail to show any major concentration of strength. In ^{16}O, for example, the (α, γ) measurements[7] over an energy range of ~8 MeV give ~17% of the isocalar energy-weighted $E2$ sum rule, while the $(\vec{p}, \gamma)$ results[4] exhaust about 30% of the isovector sum. (It should be noted that the sum rule used in Ref. 4 did not contain the factor of $\frac{3}{5}$ usually included in evaluating the quantity $\langle r^2 \rangle$. See Sec. V below.)

In the present experiment we have utilized the capture reaction $^{14}C(p, \gamma)^{15}N$ with both unpolarized and polarized proton beams to determine the $E2$ strength in ^{15}N. It will be seen that our results indicate a broadly spread $E2$ strength which, when integrated over ~12 MeV, using our most probable values, accounts for about 7.0% of the energy-weighted total $E2$ sum rule. Within the experimental uncertainty this amount could range from 2 to

64%. Our results also reveal the detailed structure and spin composition of the dominant electric dipole ($E1$) giant resonance.

II. EXPERIMENTAL DETAILS

The asymmetry data were measured using the Lamb-shift polarized ion source[8] at the Triangle Universities Nuclear Laboratory (TUNL). The polarization of the protons, determined at 20 min intervals by the quench-ratio technique,[9] was found to be essentially constant during the course of a run with a typical value of 0.80 ± 0.02. The beam current on target was in the 40–60 nA range. Measurements were obtained by running the beam alternately in the spin up and the spin down modes.

The ^{14}C targets used in these measurements were prepared at Oak Ridge National Laboratories.[10] These targets were made by cracking 90% ^{14}C enriched acetylene on thin (0.12 μm)Ni backings. The ^{14}C target thickness was measured to be about 30 μg/cm^2 by means of the ^{14}C$(p, p)^{14}$C reaction. Data were taken over the energy range of 2.1 to 2.4 MeV. The yields were normalized to the results of Harris and Armstrong,[11] and used to calculate the target thickness. The error on this number is estimated to be about 25%, coming primarily from the 20% error associated with the absolute cross section of Ref. 11. Since the yield for the ^{14}C$(p, \gamma_0)^{15}$N reaction is quite small, two targets were placed in the scattering chamber. This configuration resulted in an over-all target thickness which was measured to be 60 μg/cm^2.

A previous preliminary report of this experiment[3] was based on measurements performed with a 12.7×12.7 cm NaI crystal which was physically shielded by lead and paraffin to reduce the background counting rate. Due to the low counting rate for the ^{14}C$(p, \gamma_0)^{15}$N reaction under our experimental conditions, a major problem in this configuration was the cosmic-ray background. In order to improve the quality of the data the measurements were repeated with a new detection system installed at TUNL, which provides improved resolution and efficiency while reducing background and eliminating cosmic-ray counts.

The new detector consists of a 25.4×25.4 cm NaI crystal viewed by six RCA-8575 photomultiplier tubes, as illustrated in Fig. 1. The crystal is surrounded in front and on the sides by an anticoincidence shield of NE110 plastic in the form of a well 7.6 cm thick in front and 12.7 cm thick on the sides (see Fig. 1).[12] The shield is viewed by eight XP1031 photomultiplier tubes. The entire assembly is surrounded by 10 cm of lead, 20 cm of paraffin doped with Li_2CO_3 (about 50% by weight), and cadmium sheet to reduce the background counting rate. The front face of the crystal was positioned 56 cm from the target. The lead collimator used in the present experiment was designed so that the back face of the crystal was fully illuminated. This geometry results in a total angular acceptance of 18°.

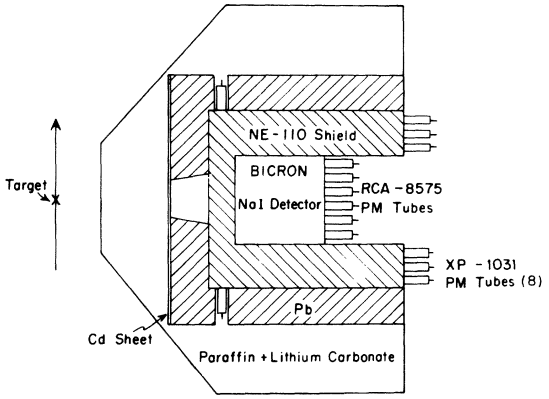

FIG. 1. Schematic diagram of the detector system.

The beam was dumped in a shielded Faraday cup positioned 3 m beyond the target. The shielding at the Faraday cup consisted of about 10 cm of lead and 70 cm of paraffin. To minimize the background from beam collimators, a single insulated collimator, set close to the target, was used. The beam current striking this collimator was monitored and kept at a minimum.

The electronic configuration is illustrated in Fig. 2. The direct anode signals from the photo multipliers on the NaI detector were added in a linear mixer. For the shield, each signal was amplified prior to mixing. The possibility of spectrum-distorting pileup events was reduced by time clipping the NaI signal and passing it through a fast linear gate (of about 250 nsec) prior to processing in a linear amplifier. The gate was then held closed

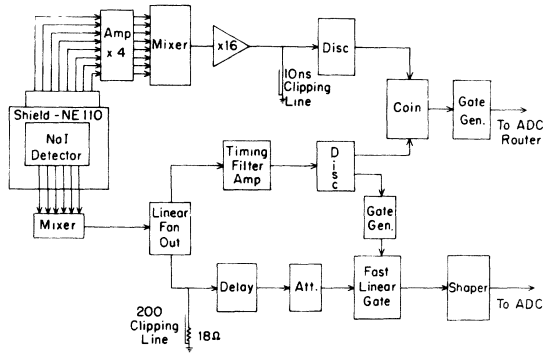

FIG. 2. Block diagram of the electronic configuration. Additional electronics used to measure the accidental rate are not shown.

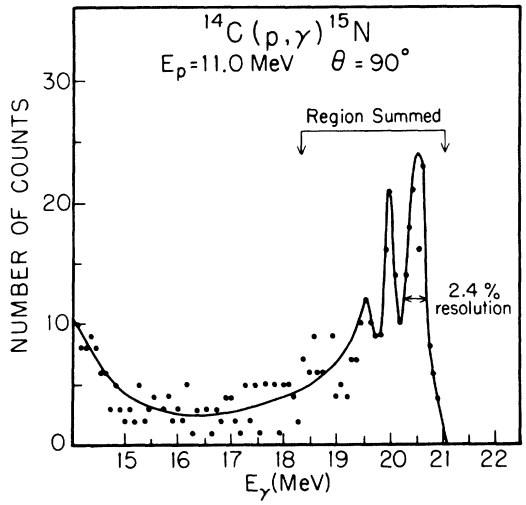

FIG. 3. The $^{14}C(p,\gamma)^{15}N$ spectrum for a proton energy of 11.0 MeV. The two escape peaks are clearly resolved.

for the signal processing time (about 10 μsec).

The resolution of the system was determined to be ~2.4% under ideal conditions. A spectrum illustrating this is shown in Fig. 3. It was found that, in practice, gain shifts related to the background counting rate made it difficult to maintain this resolution, a more typical value being about 3–4%. If the beam was run so that essentially no collimator current could be measured, the resolution improved. By keeping the total counting rate in the NaI detector below 10^5 counts per second, good resolution (3–4%) could be maintained.

The data were stored in two 512 channel spectra, one of which collected those NaI pulses which were vetoed by the shield. As seen in Fig. 3, we are not rejecting an appreciable amount of the escape peaks in this experiment. Although this could be accomplished by increasing the amplification of the shield pulses, in the present case the resolution is adequate without discarding these pulses. The cosmic ray rejection efficiency of our system was found to be about 97% under these conditions.

The efficiency of the detector system was determined by means of the $^{12}C(p,\gamma_0)$ reaction.[13] A ^{12}C target, about 45 keV thick for 14.2 MeV protons, was used to measure a yield curve over the 15.07 MeV resonance in ^{13}N. On and off resonance angular distributions were combined to obtain the integrated resonance yield. This yield, along with a recent measurement of the number of γ rays per proton $[(6.83\pm0.22)\times10^{-9}]$ (Ref. 14) was used to determine the efficiency of our detection system. The result of this measurement yielded an efficiency of $26\pm6\%$ when the peak was summed as described below. The absolute cross section for the $^{14}C(p,\gamma_0)^{15}N$ reaction were determined assuming that the efficiency would remain constant at this value for all γ-ray energies for 14–25 MeV.

III. EXPERIMENTAL RESULTS

The excitation curve of the $^{14}C(p,\gamma)^{15}N$ yield measured at $\theta=90°$ with an unpolarized beam in 100 keV steps is shown in Fig. 4. These results are in reasonably good agreement with our previously reported results,[15] although the cleaner spectra of the present experiment result in a reduction of background contamination and somewhat sharper structure. The data were converted from (p,γ) to (γ,p) cross sections using the principle of detailed balance.[16] The peak (γ,p) cross section, when integrated over angle, is 5.0 ± 1.3 mb. [The absolute cross section determined as described above has an uncertainty of $\pm25\%$.] The previously reported value for this number, obtained in the photonuclear measurements of (γ,p) cross sections, was 4.5 ± 0.7 mb[17] and is seen to be in excellent agreement with our result.

The angular distributions of unpolarized cross sections are shown in Fig. 5. In this figure we have plotted the quantity $\sigma(\theta)/a_0$. The cross section data shown are the composite results of measurements with the polarized beam and separate measurements with an unpolarized beam. The quantity a_0 will be defined below. The asymmetry measurements are presented in terms of the quantity $\sigma(\theta)A(\theta)/a_0$, where

$$A(\theta)=\frac{N_+-N_-}{N_++N_-}\frac{1}{P}$$

and N_+ is the number of counts obtained for spin up measurements, and N_- is the number in the spin down case. The error bars represent the statistical errors associated with these quantities including the error in the beam polarization P.

IV. ANALYSIS OF DATA

Since the γ ray peak corresponding to (p,γ_0) is well resolved and essentially free of background, the spectra were readily processed by simply summing the region shown in Fig. 3. The conversion of these sums to absolute cross sections has been previously discussed. The angular distributions of cross sections were fitted using a least squares criterion by an expansion in terms of Legendre polynomials

$$\sigma(\theta)=a_0\left[1+\sum_{k=1}^{3}\frac{a_k}{a_0}Q_kP_k(\cos\theta)\right],$$

with the proper statistical errors, geometrical correction factors (Q_k) resulting from the finite detector size,[18] and center of mass corrections

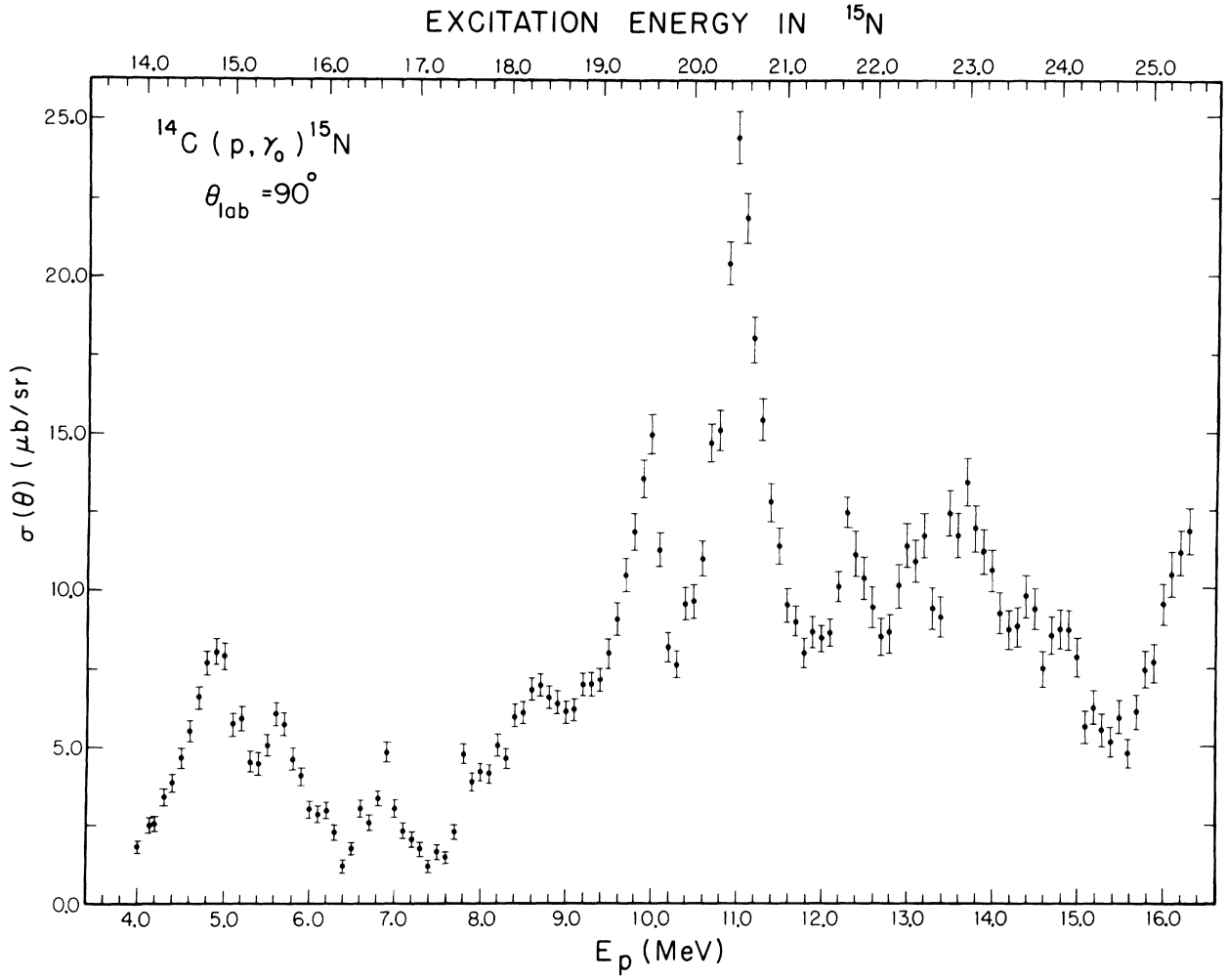

FIG. 4. The excitation curve for the $^{14}C(p,\gamma_0)^{15}N$ reaction at $\theta_{lab} = 90°$. The error bars represent the statistical errors associated with the data points.

taken into account. Similarly, the product of the analyzing power and the cross section was fitted by an expansion in associated Legendre polynomials

$$A(\theta)\sigma(\theta) = \sum_{k=1}^{3} b_k Q_k P_k^1(\theta).$$

In this procedure the normalization is taken so that a_0 is set equal to 1.0. The geometrical factors Q_k, the depolarization effects due to the azimuthal angular range, and the center of mass corrections were taken into account.

The results of the least squares fits to the data are shown as the solid lines in Fig. 5. The resulting a and b coefficients are presented in Table I for the eight measured energies. The normalized χ^2 values were used to determine the highest order terms which should be included in our fits. The data were fitted including one, two, three, and four terms (i.e., up to and including P_3 and P_4^1, respectively). The normalized χ^2 values obtained from these fits indicated that in all cases [with one possible exception (see below)] the inclusion of terms having order greater than three was not statistically justified. In some cases terms of order three (see Table I) were not required. Since, in the present case, finite b_4 coefficients could come only from $E2$-$E2$ interference, their absence is not surprising.

If we compare the values presented in Table I with those previously reported in Ref. 3, we find basic agreement, within the error bars, for measurements made at corresponding energies. The notable exception to this is at $E_p = 4.83$ MeV, where the previous data were apparently contaminated by the background. It is also interesting to note that

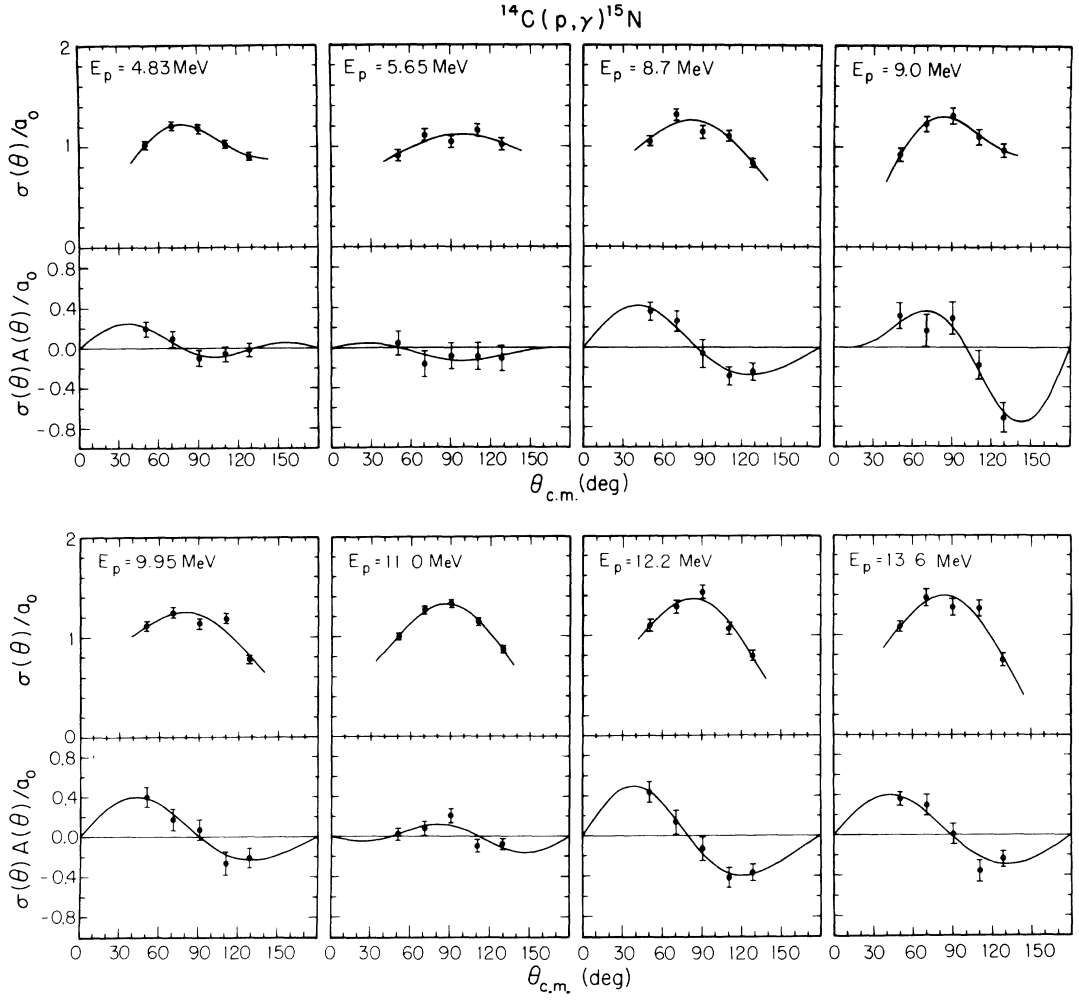

FIG. 5. The normalized cross section and cross section times analyzing power data as a function of energy and angle. The error bars represent the statistical errors associated with the data points. The solid lines are a result of the fits discussed in the text and summarized in Table I.

there is, both in the data of Ref. 3 and in the present results, some suggestion of higher order multipoles in the analyzing power measurements at $E_p = 11.0$ MeV. This is manifested in the rate of fall of the $A(\theta)\sigma(\theta)$ curve from 90° to 110°. In both measurements this rate exceeds the value obtained by fitting through b_4 only. However, data at more angles having better statistics would be required to

TABLE I. The a and b coefficients obtained by least squares fitting the data of Fig. 5 as discussed in the text. Entries of 0.0 ± 0.0 indicate that the χ^2 values implied that these terms were not required to fit the data.

E (MeV)	a_1/a_0	a_2/a_0	a_3/a_0	b_1	b_2	b_3
4.83	−0.03 ± 0.10	−0.36 ± 0.08	−0.25 ± 0.14	0.03 ± 0.04	0.07 ± 0.03	0.07 ± 0.03
5.65	−0.08 ± 0.06	−0.24 ± 0.11	0.0 ± 0.0	−0.09 ± 0.07	0.03 ± 0.05	0.03 ± 0.06
8.7	0.21 ± 0.05	−0.50 ± 0.11	0.0 ± 0.0	0.01 ± 0.05	0.23 ± 0.04	0.04 ± 0.05
9.0	−0.18 ± 0.17	−0.57 ± 0.15	−0.30 ± 0.25	−0.02 ± 0.08	0.31 ± 0.06	−0.16 ± 0.06
9.95	0.25 ± 0.05	−0.47 ± 0.10	0.0 ± 0.18	0.05 ± 0.05	0.22 ± 0.04	0.03 ± 0.05
11.0	0.11 ± 0.03	−0.65 ± 0.07	0.0 ± 0.12	0.02 ± 0.03	0.05 ± 0.02	−0.06 ± 0.03
12.2	0.27 ± 0.06	−0.71 ± 0.13	0.0 ± 0.07	−0.07 ± 0.05	0.28 ± 0.04	0.07 ± 0.05
13.6	0.26 ± 0.06	−0.77 ± 0.15	0.0 ± 0.0	0.02 ± 0.05	0.23 ± 0.03	0.03 ± 0.04

quantitatively evaluate this effect.

The resulting a and b coefficients can be related to the amplitudes of the various transition matrix elements. In the present case, states in ^{15}N which decay to the $\frac{1}{2}^-$ ground state by electric dipole ($E1$) radiation must have $J^\pi = \frac{1}{2}^+$ or $\frac{3}{2}^+$. Since the target spin is zero, the excitation of these states requires incoming protons having a j of $\frac{1}{2}^+$ or $\frac{3}{2}^+$, respectively. These two proton configurations are labeled as $s_{1/2}$ and $d_{3/2}$ and the transition matrix elements will be referred to as $s_{1/2}$ ($E1$) and $d_{3/2}$ ($E1$). At this point our approach is to introduce the minimum number of additional states having different J^π values necessary to account for our data. Once a state is determined to be necessary, we will allow it to decay whenever possible, with the restriction that it do so via $E1$, $M1$, or $E2$ radiation. Since there are finite a_3 and b_3 coefficients, we must have states present which decay via $E2$ radiation. The possible J^π values are $\frac{3}{2}^-$ and $\frac{5}{2}^-$. If we choose $\frac{5}{2}^-$, we would, in general, have finite a_4 coefficients, in contradiction to our data. It would be possible to have both $\frac{5}{2}^-$ and $\frac{3}{2}^-$ states present with amplitudes and phases which just cancel the a_4 and b_4 coefficients. This would seem unlikely to occur at all of our measured energies. The choice of $\frac{3}{2}^-$ gives a_4 and b_4 identically zero, which is consistent with the results of our data. The existence of $\frac{3}{2}^-$ states in ^{15}N also allows for the possibility of $M1$ decay. The associated T-matrix element will be denoted by $p_{3/2}$ ($M1$). Although additional $M1$ strength could originate from $\frac{1}{2}^-$ states, this has been neglected. A single-particle shell model calculation using bare nucleon g factors favors the $p_{3/2} \rightarrow p_{1/2}$ transition over the $p_{1/2}$ to $p_{1/2}$ transition by a factor of 10 for $\Delta T = 1$, and by a factor of 5 for $\Delta T = 0$ transitions. Our ability to account for the data without introducing additional states of different J^π would appear to justify these assumptions. It is now a straightforward problem to express the a and b coefficients in terms of the transition matrix elements (their amplitudes and phases). This amounts to evaluating the angular momentum coupling coefficients.

The expressions for the a and b coefficients of the present problem in terms of these transition matrix elements [$s_{1/2}(E1)$, $d_{3/2}(E1)$, $p_{3/2}(E2)$, and $p_{3/2}(M1)$] and their relative phases are given below:[19]

$$a_0 = s_{1/2}(E1)^2 + 2d_{3/2}(E1)^2 + 2p_{3/2}(E2)^2 + 2p_{3/2}(M1)^2,$$

$$a_1 = 2.0 s_{1/2}(E1)p_{3/2}(M1)\cos(s, p_1) - 2.0 p_{3/2}(M1)d_{3/2}(E1)\cos(p_1, d) + 3.464 s_{1/2}(E1)p_{3/2}(E2)\cos(s, p_2) + 0.693 d_{3/2}(E1)p_{3/2}(E2)\cos(d, p_2),$$

$$a_2 = -2.0 s_{1/2}(E1)d_{3/2}(E1)\cos(s, d) - p_{3/2}(M1)^2 - d_{3/2}(E1)^2 + 3.464 p_{3/2}(E2)p_{3/2}(M1)\cos(p_2, p_1) + p_{3/2}(E2)^2,$$

$$a_3 = -4.157 d_{3/2}(E1)p_{3/2}(E2)\cos(d, p_2),$$

$$b_1 = -1.0 s_{1/2}(E1)p_{3/2}(M1)\sin(s, p_1) - 4.0 p_{3/2}(M1)d_{3/2}(E1)\sin(p_1, d) + 1.386 d_{3/2}(E1)p_{3/2}(E2)\sin(p_2, d) - 1.732 s_{1/2}(E1)p_{3/2}(E2)\sin(s, p_2),$$

$$b_2 = -s_{1/2}(E1)d_{3/2}(E1)\sin(s, d),$$

$$b_3 = -1.386 d_{3/2}(E1)p_{3/2}(E2)\sin(p_2, d),$$

where $(s, p) = \phi_s - \phi_p$, $(p, d) = \phi_p - \phi_d$, $(s, d) = \phi_s - \phi_d$, and ϕ_{p_1} and ϕ_{p_2} refer to the $p_{3/2}(M1)$ and $p_{3/2}(E2)$ matrix elements, respectively.

The equations emphasize a fundamental difference between the present experiment and previous similar experiments. This is the fact that, since we have a spin zero target, the analyzing power will be identically zero if we form a single state of definite J^π. This is distinctly different from previously reported results,[1,2] where pure $E1$ radiation from a state of definite J^π, which was formed by two l values, produced a large analyzing power. The large analyzing powers obtained in the present experiment indicate that, in general, the J^π values are not pure at a given energy of the giant dipole resonance region of ^{15}N.

The unknowns of this problem are the four amplitudes and the three phases [the $p(E2)$ and $p(M1)$ phases are either taken to be equal or to differ by 180° in our analysis].[20] Therefore, since one phase can be chosen arbitrarily, there are only two parameters required to describe the phases [say $(\phi_p - \phi_d)$ and $(\phi_s - \phi_d)$]. We are, therefore, left with the problem of having six unknowns and seven equations.

The procedure used to find the solutions to these equations which agree with the experimental coefficients of Table I was as follows. The ampli-

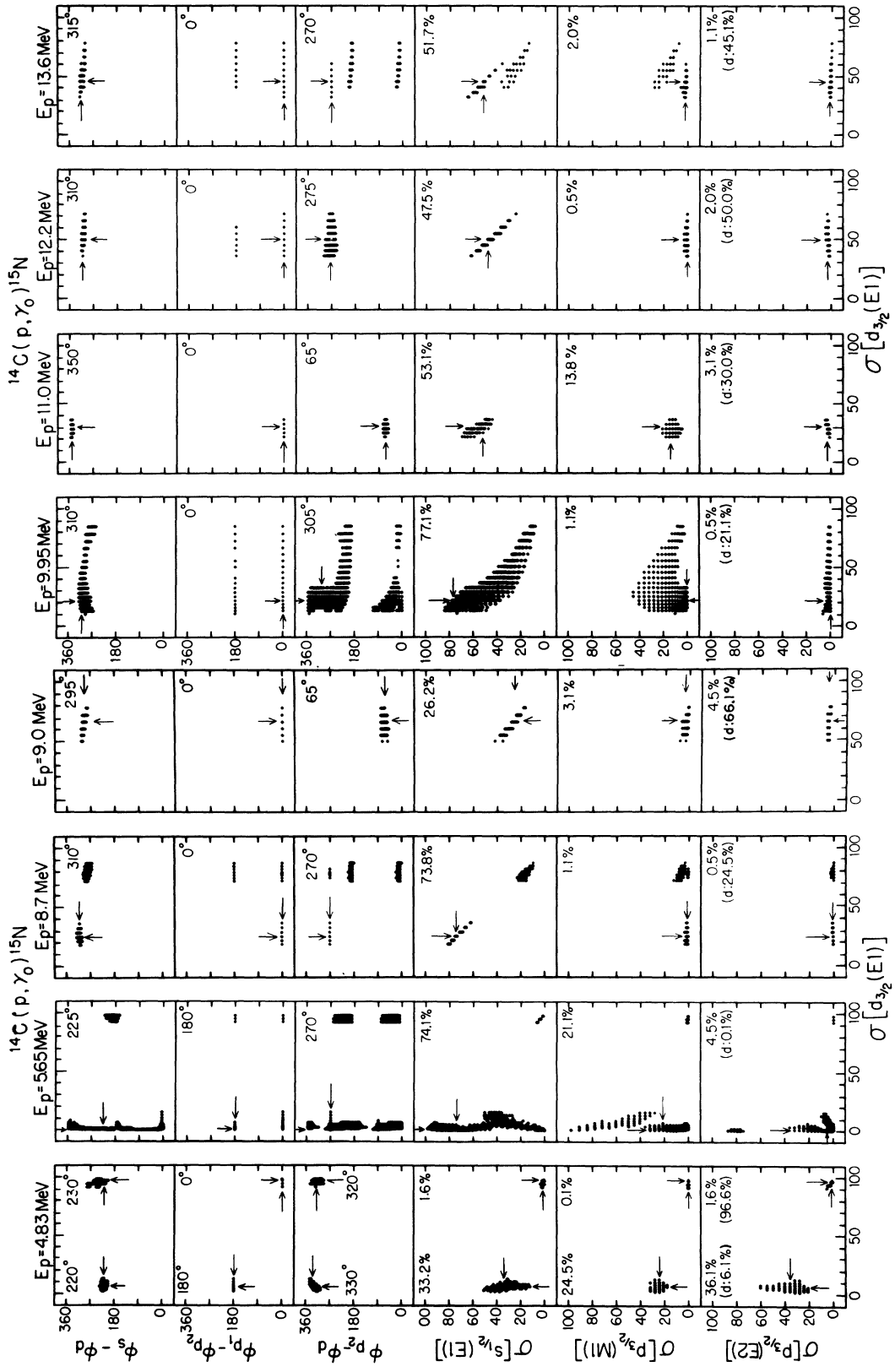

FIG. 6. The solutions to the equations in the text for the amplitudes and phases which are allowed by the coefficients of Table I. The amplitudes have been converted to percentage cross sections. The best χ^2 values are indicated by the arrows and tabulated in figure.

tude parameters were stepped in increments of 0.025 over their full allowed range (consistent with all of the equations). The two phase angle differences were stepped in increments of 5.0° over the full range of 0° to 360° and the two p phases were allowed either to be equal or to differ by 180°. Each solution was checked by the computer to see if the calculated a and b coefficients were within the error bars of the experimental values. In addition, the value of χ^2 was calculated for each solution. The resulting solutions at a given energy were plotted as shown in Fig. 6, where we have plotted the percentage of the cross section (i.e., the fraction of a_0) due to each transition amplitude as a function of the percentage which is due to $d_{3/2}(E1)$ for each measured energy. The phase differences are also shown. The result which corresponds to the solution which has the best χ^2 value is indicated. As readily seen in this figure, the solutions display a "smear" due to the errors in the experimentally determined coefficients.

In the procedure of requiring that each solution reproduce all of the coefficients within their errors, we are omitting some solutions which may have χ^2 values less than some of those obtained. However, our best χ^2 values are all less than 1—and for $\chi^2 < 1$ we have not missed any solutions with the present criteria. At one energy ($E = 9.0$ MeV) we found that the best χ^2 value was slightly greater than 1. To investigate this we performed our calculations again, allowing each calculated coefficient to deviate from the experimental values by the number of standard deviations equal to the smallest χ^2 value previously found. No new solutions having better χ^2 values were found. Finally, in regions in which a small island of solutions was found (see Fig. 6), a finer grid step of 0.01 was used to assure us that the full range of solutions had been found. No significant new solutions were found when this was done, a result which helped assure us that we had taken sufficiently small steps in finding solutions.

As indicated in Fig. 6, there are two best χ^2 solutions at $E_p = 4.83$ MeV. One of these has a small $d_{3/2}(E1)$ strength, but considerable $p_{3/2}(E2)$ strength (36.1%). The other is almost pure $d_{3/2}(E1)$. In general, the $E1$ strength from $s_{1/2}$ and $d_{3/2}$ amplitudes, respectively, does not show any apparent systematic behavior as a function of energy. We do observe that from 10 MeV up to 14 MeV the $s_{1/2}(E1)$ strength accounts for about 50% of the cross section.

The $p_{3/2}(E2)$ strength is of special interest since it could indicate the possible existence of an $E2$ giant resonance[4] in this energy range. At 5.65 MeV we see two basic solutions, one of which allows a large $E2$ strength (about 87%). Since the statistics on the 5.65 MeV data are especially bad, and since the 87% result at this energy is so anomalous, we feel that this result should be ignored. At the higher energies, however, the maximum $E2$ strength is typically only about 2–6% of the cross section. More will be said about the implications of these results later.

The $p_{3/2}(M1)$ strength must be finite at only two of the eight energies. The cross section at 4.83 MeV is at least 21% $p_{3/2}(M1)$ for the solution with appreciable $E2$ strength, although it can be essentially zero for the solution dominated by $d_{3/2}(E1)$. At 11 MeV the smallest value for this strength is 4.5%. At the other energies the $p_{3/2}(M1)$ strength could be essentially zero. At these energies we could have acceptable solutions if the $M1$ decay were omitted. However, our results at 4.85 and 11 MeV indicate that a blanket assumption[4] that the $M1$ strength will be negligible may not always be valid.

The relative phases between the various amplitudes appear to be quite energy dependent. The spread in the allowed values shown in Fig. 6 reflects the error in the experimentally determined coefficients. In the case of $(\phi_s - \phi_d)$ the best χ^2 value varies as a function of energy between 220° and 350°. A much broader range of values is seen in the case of $\phi_p - \phi_d$ for which the best χ^2 value varies from 65° to 330° over the energy region studied. As indicated in Fig. 6, the solutions which correspond to the best χ^2 values are, with the exception of the 5.65 MeV case, all consistent with $\phi_{p1} = \phi_{p2}$.

V. SUM RULES AND CONCLUSIONS

The $p_{3/2}(E2)$ strength displayed in Fig. 6 can be used to evaluate the percentage of the energy-weighted $E2$ sum rule observed in this experiment. The sum rule for $E2$ radiation can be written either for a change of isospin ($\Delta T = 1$), for no change ($\Delta T = 0$), or for both. Since the present experiment allows for both, we shall compare the observed strength to all three sum rules. The appropriate sum rules are[21]:

$$\Delta T = 1: \int \frac{\sigma_{E2}(\gamma, x)}{E^2}\, dE \cong 2.4 \times 10^{-4} \frac{NZ}{A^{1/3}} \text{ mb MeV}^{-1}$$

$$= 54.5 \text{ mb MeV}^{-1},$$

$$\Delta T = 0: \int \frac{\sigma_{E2}(\gamma, x)}{E^2}\, dE \cong 2.4 \times 10^{-4} \frac{Z^2}{A^{1/3}} \text{ mb MeV}^{-1}$$

$$= 47.7 \text{ mb MeV}^{-1},$$

Total: $\int \frac{\sigma_{E2}(\gamma, x)}{E^2} dE \cong 2.4 \times 10^{-4} ZA^{2/3}$ mb MeV^{-1}

$= 102.2$ mb MeV^{-1} .

In order to integrate the $E2$ strength of Fig. 6, the percent cross sections were first converted to absolute cross sections and then, using the principle of detailed balance, to (γ, p) cross sections. The maximum value, minimum value, and the value of the $E2$ strength which corresponded to the best χ^2 value at each energy was used to construct a histogram over the energy range of the experiment as shown in Fig. 7.

The results of integrating these three strengths are presented in Table II as the percentages of the three sum rules. In the case of the maximum values we find that if we use the maximum values of Fig. 7 we obtain 64% of the total energy-weighted $E2$ sum rule. The histogram of Fig. 7 does not include the 85% result at 5.65 MeV.

The result of this experiment allows for an $E2$ strength in the region of ^{15}N from 14.3 to 23.3 MeV which exhausts a maximum of 64% of the total energy-weighted $E2$ sum rule, a minimum of 2.1% and a most probable value of 28% or 7%. This latter most probable result is double valued due to the fact that there are two solutions which have the best χ^2 value at 4.83 MeV (36.1% and 1.6%, respectively). If we assume that a similar amount of $E2$ strength would be found in the neutron channel, then the most probable value would exhaust about 56 or 14% of the total energy weighted $E2$ sum rule. Since the higher value here arises from an isolated solution at one energy, it is less credible than the lower value. Hence we conclude that the "*most* probable value" should be taken to be 14%. While these results allow for the existence of a "giant" $E2$ resonance, the "*most* probable value" indicates that no appreciable concentration of $E2$ strength is observed in ^{15}N over the energy region studied.

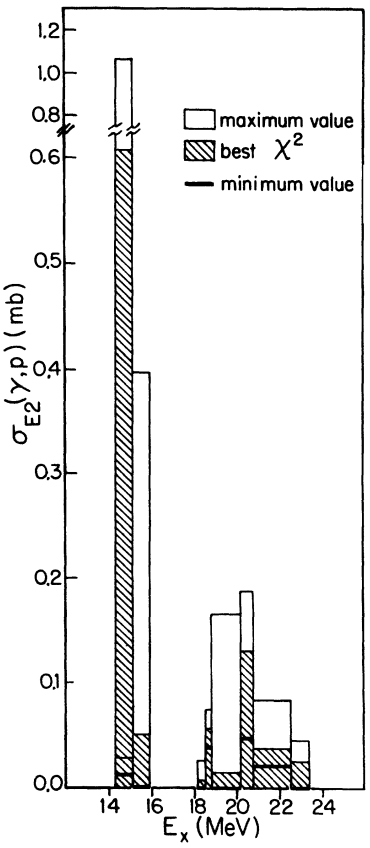

FIG. 7. The E_2 cross section found in the present experiment presented as $\sigma(\gamma,p)$. The minimum, maximum, and best χ^2 values are shown. Note that the E_x = 14.7 MeV region has two best χ^2 values.

TABLE II. The percentage of the energy-weighted $E2$ sum rules observed in this experiment.

Sum rule	% of Sum rule Minimum	Maximum	Best χ^2
$\Delta T = 1$	3.9%	120%	13.2% (52.6%)
$\Delta T = 0$	4.5%	137%	15.1% (60.1%)
Total	2.1%	63.8%	7.0% (28.0%)

A similar procedure can be applied to the $E1$ strengths. In this case, if we use the $s_{1/2}(E1)$ plus the $d_{3/2}(E1)$ strengths and construct a histogram following the procedures used in the $E2$ case, we find that the best χ^2 values yield $\int \sigma_{E1}(\gamma,p)dE$ = 13.2 MeV mb. The classical dipole sum rule[16] can be written as

$$\int \sigma_{E1}(\gamma,x)dE = 60\,\frac{NZ}{A}\ \text{MeV mb} = 224\ \text{MeV mb}\ ,$$

so we see that we have observed only about 6% of the $E1$ sum rule in the present experiment. The result obtained above compares well with the value of 14.9 MeV mb obtained in Ref. 16 for the integrated photoproton production cross section for ground state transitions up to 24.6 MeV.

VI. $E1$ STRENGTHS AND THE SHELL MODEL

In the past, a large number of shell-model studies (as well as studies involving other nuclear models) have been employed to describe the properties of the giant dipole resonance (GDR) region. These shell-model calculations have been based on a particle-hole description in which the states that make up the GDR differ from the ground state in that one particle has been excited to the next available ma-

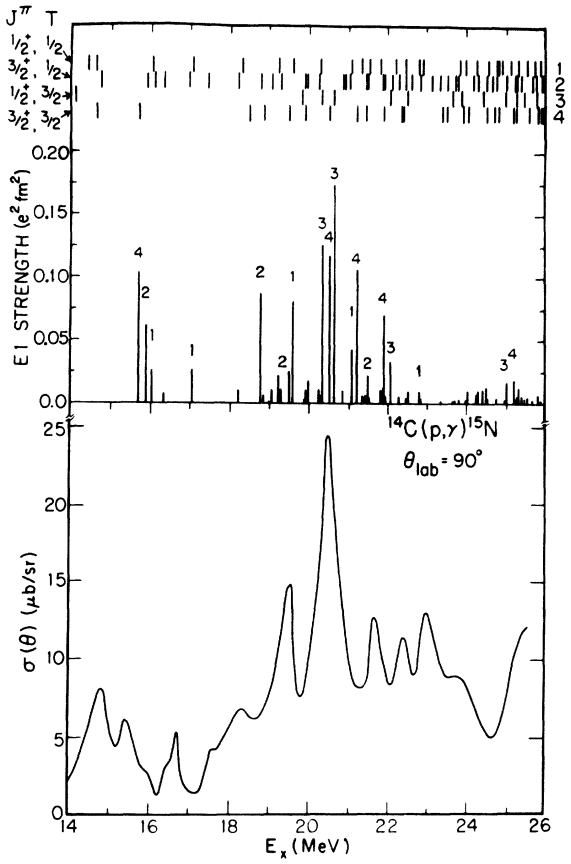

FIG. 8. The results of the shell-model calculation of $E1$ reduced strengths are shown along with the 90° yield curve for the $^{14}C(p,\gamma_0)^{15}N$ reaction. The upper lines indicate the existence of eigenstates at these energies with the quantum numbers shown—some of these states have negligible $E1$ strength and therefore do not appear on the lower part. The vertical lines of appreciable strength are labeled to make their identification (J^π, T) convenient.

jor shell of opposite parity. A representative calculation of this type has been reported by Gillet and Vinh Mau.[22] A study along similar lines has been performed for the $A = 15$ GDR by Fraser, Garnsworthy, and Spicer.[23] It should also be noted that Divadeenam and Weller[24] predicted elastic proton widths of the $A = 15$ GDR using the doorway state mechanism and diagonalizing in the configuration space of the above mentioned particle-hole description.

The present shell-model calculation differs from the previous attempts in that a much larger configuration space has been included. In addition to the usual 1p-1h excitations, most 3p-3h excitations have been included as well. No such calculation has been previously reported in the GDR region.

The six lowest shell-model orbitals have been included in the present calculation. No attempt has been made to calculate the absolute binding energies. The calculated spectrum, as shown in Fig. 8, has been normalized to the $E_x = 11.7$ MeV, $J^\pi = \frac{1}{2}^+$ analog state in ^{15}N. The relative single-particle energies adopted are -36.8, -20.8, -10.2, -6.7, -7.8, and -2.0 MeV for the $0s_{1/2}$, $0p_{3/2}$, $0p_{1/2}$, $0d_{5/2}$, $1s_{1/2}$, and $0d_{3/2}$ orbitals, respectively. A modified surface delta interaction (MSDI) has been chosen for the two-body residual interaction.[25] The choice of such a simple Hamiltonian is not felt to be a serious drawback since it has been found that most reasonable two-body interactions produce results of essentially the same quality.[26] The present MSDI parameters are taken to be: $A_0 = 0.77$, $A_1 = 0.95$, $B_0 = 2.50$, and $B_1 = 0.37$—all expressed in MeV.[27] The configuration space for the $J^\pi = \frac{1}{2}^+, \frac{3}{2}^+$, $T = \frac{1}{2}, \frac{3}{2}$ states includes all possible 1p-1h excitations as well as all 3p-3h excitations with the exception that only one hole is allowed in the $0s_{1/2}$ shell and only one particle in the $0d_{3/2}$ shell. Only $1\hbar\omega$ excitations are considered. The $(J^\pi, T) = (\frac{1}{2}^-, \frac{1}{2})$ ground state of ^{15}N is described by 0p-0h and 2p-2h excitations, but again with the previously mentioned restrictions regarding the $0s_{1/2}$ and the $0d_{3/2}$ shells. These restrictions have been applied in order to make the matrix sizes manageable.

The usual effective charges $\epsilon_p = N/A$ and $\epsilon_n = -Z/A$ have been used in calculating the reduced $E1$ transition probabilities in order to take account of the recoil of the nucleus. No attempt was made to remove the spurious states from the calculated eigenstates. It has, however, been shown by Easlea[28] that the spurious components are negligible in the GDR region.

The results of the calculations of the ground state $E1$ transitions are shown together with the 90° yield curve of the present experiment in Fig. 8. Although the experimental cross section in Fig. 8 is not directly comparable with the calculated $E1$ reduced strengths, a necessary condition to observe a resonance is that it has a reasonably large radiative width. Indeed, there is a striking correlation between the calculated strength function and the measured cross section. It also appears that the agreement is better than obtained in previous 1p-1h calculations. (One should remember that the widths on the high energy side of Fig. 8 will be enhanced by a factor of $E_\gamma{}^3$.)

The present calculation indicates that large $E1$ strengths are concentrated in a relatively few states with mainly 1p-1h character, although they are more spread out than suggested by previous 1p-1h calculations. The strength of the $T = \frac{1}{2}$, $E1$

resonances is found to be much more spread out than the $T=\frac{3}{2}$ strength which starts around 16 MeV. The distribution of $E1$ reduced strength for the $T=\frac{1}{2}$ states is predicted to be 21, 55, and 24% in the region below 15 MeV, in the region from 15–26 MeV, and in the region above 26 MeV, respectively. The corresponding percentage numbers for the $T=\frac{3}{2}$ states are 1, 74, and 25. It is also clear that the calculation predicts a general intermingling of $J^\pi=\frac{1}{2}^+$ and $\frac{3}{2}^+$ states, a result which agrees with the analysis of Sec. IV. Therefore, it does not seem very meaningful to discuss the isospin-spin splitting of the different states in this case.

An energy-weighted sum of the present shell-model results for the $E1$ reduced strengths gives

$$\sum_{E_f=15\text{–}26\ \text{MeV}} B(E1)(E_f - E_i) = 44.2\ \text{MeV}\ e^2\text{fm}^2.$$

The classical sum rule[21] expressing the same sum yields a value of 55.5 MeV e^2fm^2.

In order to obtain a more stringent test of the present wave functions, it would be desirable to calculate the proton widths in the GDR region. An effort to combine the large shell-model codes with codes to calculate the particle widths in the doorway state formalism is underway in this laboratory.

The authors wish to thank Mr. D. Griggs and Mr. G. Rochau for their help in obtaining these data. We are also indebted to Dr. T. B. Clegg for his generous help and advice in operating the TUNL polarized ion source. We gratefully acknowledge helpful discussions with Dr. L. C. Biedenharn.

---

*Work partially supported by the Research Corporation.
†Work partially supported by the National Science Foundation.
‡Work partially supported by the U.S. Energy Research and Development Administration.

[1]S. S. Hanna, H. F. Glavish, E. M. Diener, J. R. Calarco, C. C. Chang, R. Avida, and R. N. Boyd, Phys. Lett. 40B, 631 (1972).
[2]H. F. Glavish, S. S. Hanna, R. Avida, R. N. Boyd, C. C. Chang, E. Diener, Phys. Rev. Lett. 28, 766 (1972).
[3]H. R. Weller, N. R. Roberson, D. Rickel, C. P. Cameron, R. D. Ledford, T. B. Clegg, Phys. Rev. Lett. 32, 177 (1974).
[4]S. S. Hanna, H. F. Glavish, R. Avida, J. R. Calarco, E. Kuhlmann, R. LaCanna, Phys. Rev. Lett. 32, 114 (1974); and E. Kuhlmann, E. Ventura, J. R. Calarco, D. G. Mavis, and S. S. Hanna, Phys. Rev. C 11, 1525 (1975).
[5]G. R. Satchler, Phys. Rep. 14C, 99 (1974), and references contained therein.
[6]J. M. Moss, C. M. Roysa, J. D. Bronser, and D. H. Youngblood, Phys. Lett. 53B, 51 (1974).
[7]K. A. Snover, E. G. Adelberger, and D. R. Brown, Phys. Rev. Lett. 32, 1061 (1974).
[8]T. B. Clegg, G. A. Bissinger, W. Haeberli, and P. A. Quin, in *Polarization Phenomena in Nuclear Reactions*, edited by H. H. Barschall and W. Haeberli (Univ. of Wisconsin Press, Madison, Wisconsin, 1970), p. 835.
[9]T. A. Trainor, T. B. Clegg, and P. W. Lisowski, Nucl. Phys. A220, 533 (1974).
[10]Oak Ridge National Laboratories, Isotope Sales, Oak Ridge, Tennessee.
[11]W. R. Harris and J. C. Armstrong, Phys. Rev. 171, 1230 (1968).
[12]M. Suffert, W. Feldman, J. Mahieux, and S. S. Hanna, Nucl. Instrum. Methods 63, 1 (1968).
[13]F. S. Dietrich, M. Suffert, A. V. Nero, and S. S. Hanna, Phys. Rev. 168, 1169 (1968).
[14]R. E. Mans, E. G. Adelberger, K. A. Snover, and M. D. Cooper, Phys. Rev. Lett. 35, 202 (1975).
[15]H. R. Weller, R. A. Blue, J. J. Ramirez, and E. M. Bernstein, Nucl. Phys. A107, 177 (1973); A185, 284 (1972).
[16]See, for example, Evans Hayward, in *Nuclear Structure and Electromagnetic Interactions*, edited by N. McDonald (Plenum, New York, 1965), p. 141.
[17]J. L. Rhodes and W. E. Stephens, Phys. Rev. 110, 1415 (1958); R. Kosiek, Z. Phys. 179, 544 (1964).
[18]A. J. Ferguson, *Angular Correlation Methods in Gamma-Ray Spectroscopy* (North-Holland, Amsterdam, 1965).
[19]H. F. Glavish (private communication).
[20]H. Fraunfelder and R. M. Steffen, in *Alpha-, Beta-, and Gamma-Ray Spectroscopy*, edited by K. Siegbahn (North-Holland, Amsterdam, 1965), Vol. 2, p. 1020; L. C. Biedenharn (private communication).
[21]M. Gell-Mann and V. L. Telegdi, Phys. Rev. 91, 169 (1953) [see also O. Nathan and S. G. Nilsson, in *Alpha-, Beta-, and Gamma-Ray Spectroscopy*, edited by K. Siegbahn (see Ref. 20), Chap. X].
[22]V. Gillet and N. Vinh Mau, Phys. Lett. 1, 25 (1962).
[23]R. F. Fraser, R. K. Garnsworth, and B. M. Spicer, Nucl. Phys. A156, 489 (1970).
[24]M. Divadeenam and H. R. Weller, Phys. Rev. Lett. 33, 1359 (1974).
[25]R. Arvieu and S. A. Moszkowski, Phys. Rev. 145, 830 (1966); P. W. M. Glaudemans, P. J. Brussard, and B. H. Wildenthal, Nucl. Phys. A102, 593 (1967).
[26]J. B. McGrory, in *The Two-Body Force in Nuclei*, edited by S. M. Austin and G. M. Crawley (Plenum, New York-London, 1972), p. 183.
[27]B. H. Wildenthal and J. B. McGrory, Phys. Rev. C 7, 714 (1973).
[28]B. R. Easlea, Phys. Lett. 1, 163 (1962).